Daniel Rodríguez · Vassilis Theofilis

On the birth of stall cells on airfoils

Abstract Critical point theory asserts that two-dimensional topologies are defined as degeneracies and any three-dimensional disturbance of a two-dimensional flow will lead to a new three-dimensional flowfield topology, regardless of the disturbance amplitude. Here, the topology of the composite flowfields reconstructed by linear superposition of the two-dimensional flow around a stalled airfoil and the leading stationary three-dimensional global eigenmode has been studied. In the conditions monitored the two-dimensional flow is steady and laminar and is separated over a fraction of the suction side, while the amplitudes considered in the linear superposition are small enough for the linearization assumption to be valid. The multiple topological bifurcations resulting have been analysed in detail; the surface streamlines generated by the leading stationary global mode of the separated flow have been found to be strongly reminiscent of the characteristic *stall cells*, observed experimentally on airfoils just beyond stall in both laminar and turbulent flow.

Keywords Stall cells · Flow topology · Global flow instability

1 Introduction

When a plane rectangular wing is pitched up to angles of attack just beyond stall, the separated flow on the suction side is organized into three-dimensional structures known in the literature as *stall cells*, *owl-face* structures or *mushrooms*. Oil and smoke visualization techniques have been used in order to recover experimental evidence of these structures both on two-dimensional airfoils and on finite-wing models (see, e.g. Bippes and Turk [4]). Furthermore, the emergence of the stall cells was shown not to be a tip effect [21,30], but the result of a periodic spanwise breakdown of the separated region. Based on their experimental observations, Winkelmann and Barlow [30] proposed a model of the time-averaged structure of the stall cells, in which the counter-rotating swirl patterns in the oil flow are produced by the effect of a vortex connecting the two foci on the surface. A physical origin for this model was proposed by Weihs and Katz [29]. The latter authors suggested that the pure two-dimensional vortex system of the separated flow is unstable, leading to a spanwise waviness of the vortex cores which eventually hit the airfoil surface. This process results in the formation of multiple time-averaged vortex rings which induce the *owl-face* structures observed. However, in a later article, Yon and Katz [31] showed that the "tentative flow model" of Winkelmann and Barlow [30] with a vortex core impinging on the focal points at the surface was not consistent with the measured pressure distributions in the different cross-sections of the stall cells. In turn, they argued that if such vortices trail downstream, the induced flowfield would be in perfect agreement with their measurements. Moreover, Yon and Katz [31] discussed the unsteady

Communicated by T. Colonius

D. Rodríguez (✉) · V. Theofilis
School of Aeronautics, Universidad Politécnica de Madrid
Pza, Cardenal Cisneros 3, 28040 Madrid, Spain
E-mail: dani@torroja.dmt.upm.es

behaviour of the flow by means of unsteady pressure measurements. In addition to the relatively fast (Strouhal number $St \approx 0.15$) oscillations, related to the wake instability, they found large amplitude, low frequency pressure ($St \approx 0.04$) oscillations within the stall cells, while the flow outside of the cells was relatively steady. They indicated that none of this periodic behaviour were causally related to the cellular pattern, as the stall cells remain independent of the pressure fluctuations recorded on the model surface. In addition, they cited a three-dimensional numerical simulation of a rectangular wing in which multiple separation cell patterns were reproduced, while the calculations were steady, supporting the observation that unsteady shear-layer phenomena are not required for the stall cell formation. A recent direct numerical simulation study by Taira and Colonius [23] elaborates on the interplay between unsteadiness and stall cell formation; these results will not be discussed here due to the disparity of aspect ratios considered by Taira and Colonius [23] and those on which this study and the associated experiments [29–31] focus.

Turning to critical point theory, its main concepts emerged in the context of fluid flow in the early 1980s of last century [8] and it rapidly became a powerful tool in describing flow patterns in both laminar and turbulent flow. The fundamentals of the reconstruction and classification of separated flow topologies are illustrated in [9,12,17,18]. Far from reaching completion, the application of critical point concepts to the study of flow patterns, and in particular to three-dimensional separated flow, is still an active field of research [22]. Topological analysis techniques based on the description of critical points have been employed in order to characterize the flow field associated with the stall cells [8,28]. To date, different topological descriptions (i.e. characterization of the critical points and connecting streamlines) associated with separated flows may be found in the literature; however, consensus exists in the description of stall cells as symmetric counter-rotating swirling structures.

Flow instability is known to play a decisive role in configurations where laminar separation exists. Concurrently with the emergence of global instability ideas, either in its interpretation as absolute instability of weakly non-parallel flows [6,11,13] or as linear modal instability of strongly non-parallel flows [24,26], analyses of instability of laminar separation bubbles on a flat plate boundary layer have been performed. Absolute/convective instability analysis of detached boundary layers has shown the existence of a strong two-dimensional instability, related to the shear-layer [2]; in the same analysis context, the potential of self-excitation of the laminar separation bubble has also been demonstrated [11]. On the other hand, solution of the pertinent partial-derivative eigenvalue problems, without resort to the assumption of weak non-parallelism, has provided unequivocal demonstrations of the self-excitation potential of recirculating flows both in the form of laminar separation bubbles on flat surfaces [24,26] and closed recirculation regions behind geometric discontinuities [3]. The two key identification characteristics of the self-excitation instability mechanism, namely its stationary and three-dimensional nature, serve as criteria to differentiate it from the shear-layer (Kelvin–Helmholtz) instability. Hereafter, the former instability is referred to as the global mode of laminar separation bubbles.

A common characteristic of linear global (BiGlobal) instability analyses of separation bubbles is the consideration of a two-dimensional basic state with two-dimensional or three-dimensional small-amplitude disturbances superimposed, the amplitude functions of the latter being two-dimensional functions of the streamwise and wall-normal spatial coordinates. According to critical point theory, the description of the basic flow is defined as a degeneracy, only valid in the limit of strictly two-dimensional flows. The presence of the three-dimensional global mode of the separation bubble is therefore expected to give rise to new three-dimensional flow topologies, *regardless of the disturbance amplitude*. The different topological bifurcations arising from the linear superposition of a flat plate boundary-layer flow with an embedded laminar separation bubble and its leading global mode have been discussed in [20]. There, it was shown that for disturbance amplitudes small enough to remain linear, the amplification of the stationary global mode leads to the well-known *U-separation* pattern, first introduced in the literature in work classifying separated flow from a topological point of view [12]. In addition, counter-rotating structures associated with the three-dimensionality of the global mode appear in the surface streamlines, reminiscent of the stall cells observed experimentally. However, the approximation of an airfoil at a high angle of attack as a semi-infinite flat plate is bound to fail downstream of the separation bubble, as no trailing edge exists in the flat plate geometry. The trailing edge on the airfoil is itself an additional separation line, and supports critical points that can not exist in the flat plate. The no-slip condition on the airfoil surface imposes that the trailing edge be a stagnation point, from which the flow separates, also known as the Kutta condition. The trailing edge is then an additional separation line supporting new critical points which are not present in flat plate. Consequently, any attempt to identify stall cells with amplification of global modes of separation must take into account airfoil geometries, so that the Kutta condition be enforced.

In this contribution the surface streamline topology resulting from the leading amplified global mode of separated flow over a complete airfoil is discussed. In addition to the critical points known from the flat plate

analysis [20], new critical points appear on the suction side of the stalled airfoil, partly as an effect of the presence of the trailing edge. New topology bifurcations are possible then, as the critical points merge and disappear with increasing disturbance amplitudes. This article is organized as follows. The BiGlobal instability problem and the basic flow considered are presented in §2, together with some remarks on the critical point theory, included here for completeness. Results are presented in §3, with special emphasis placed on the different topologies emerging from the superposition of the global mode to the basic flow. A brief summary of the new findings and a comparison with the topologies and models found in the literature are presented in §4.

2 Theory

2.1 Global instability analysis

In the scope of a BiGlobal instability analysis [25] of the flow monitored, the unsteady total field $\mathbf{q} = (u, v, w, p)^T$ here considered incompressible, is decomposed into a steady two-dimensional basic state $\bar{\mathbf{q}}(x, y)$, with three-dimensional perturbations $\hat{\mathbf{q}}(x, y) \exp[\mathrm{i}(\beta z - \omega t)]$ superimposed:

$$\mathbf{q}(x, y, z, t) = \bar{\mathbf{q}}(x, y) + \varepsilon \hat{\mathbf{q}}(x, y) \exp[\mathrm{i}(\beta z - \omega t)]. \tag{1}$$

The amplitude of the perturbations ε is taken to be small compared to that of the basic flow, thus permitting linearization of the Navier–Stokes equations. A partial-differential-equation-based eigenvalue problem of the form

$$-\mathrm{i}\omega \mathcal{B} \cdot \hat{\mathbf{q}} = \mathcal{A}(\bar{\mathbf{q}}; \beta, Re) \cdot \hat{\mathbf{q}} \tag{2}$$

is then obtained at each Re value for the complex eigenvalue ω, taking the spanwise wavenumber β to be a real parameter, associated with the spanwise periodicity length, L_z, via $\beta = 2\pi/L_z$. The structure of the linear operators $\mathcal{A}$ and $\mathcal{B}$ can be found in [14]. A conformal mapping is introduced in order to map the geometry of the airfoil from the Cartesian coordinate system Oxy to the orthogonal curvilinear coordinates $O\xi_1\xi_2$. The linearized Navier-Stokes equations are projected on the orthonormal basis defined by the vectors

$$\mathbf{a}_k = \frac{1}{h_k} \left(\frac{\partial x}{\partial \xi_k}, \frac{\partial y}{\xi_k}, \frac{\partial z}{\partial \xi_k} \right)^T, \tag{3}$$

where $h_k = \sqrt{(\partial x/\partial \xi_k)^2 + (\partial y/\partial \xi_k)^2 + (\partial z/\partial \xi_k)^2}$ are the metric functions. Taking into account that the transformation is plane, $\xi_3 = z$ and $h_3 = 1$, and the other metric functions h_1, h_2 are independent of z. The velocity vector written in curvilinear coordinates is $\mathbf{v} = (v_1, v_2, v_3)^T$, where $v_3 = w$, the spanwise velocity component.

Chebyshev and Fourier polynomials are used, respectively, in the discretization of the wall-normal (ξ_2) and azimuthal (ξ_1) directions, the latter discretized using an O-type grid. Vanishing of the disturbance velocity components is imposed at the wall, where a compatibility boundary condition is also used for the pressure perturbation. Linear extrapolation of information within the domain is imposed as the boundary condition at the far-field. The matrix obtained from the discretization of $\mathcal{A}$ is treated as dense, is stored and operated upon using linear-algebra software on distributed memory supercomputers. The near-diagonal structure of $\mathcal{B}$, the elements of which are all zero except some of them in the diagonal which are equal to unity, permits avoiding its storage. A massively parallel implementation of the Arnoldi algorithm is used in order to recover a window of the eigenspectrum which contains the physically-interesting most unstable/least stable eigenvalues. Implementation details of the parallel solution algorithm may be found in [19].

2.2 The basic flow

The two-dimensional steady flow around an airfoil at angle of attack $\alpha = 18°$, and with Reynolds number based on the chord equal to $Re = 200$ is used as the basic flow. For the computation of the basic flow the incompressible version of the unstructured finite-volume solver *CDP*, developed at the Stanford Center for Turbulent Research, was used [14]. The Jukowski airfoil closest to a NACA0015 airfoil was considered, selected in order to obtain an exact match of the airfoil surface with the curvilinear coordinates used in the BiGlobal instability analysis. Further information on the interpolation of the basic flows from the finite volumes grid to

the structured grid used for the instability analysis, as well as the conformal mapping processes, alongside the pertinent resolution studies, have been presented elsewhere [14]. The $Re = 200$ Reynolds number and 18° angle of attack are selected in order to obtain a steady laminar solution of the two-dimensional Navier–Stokes equations, in the range in angle of attack for which stall cells have been observed experimentally.

2.3 No-slip critical points and surface streamlines

In the following, a brief summary of critical point theory [7–9,12,15,17,18] is provided for completeness. The organized structures in a flow field can be characterized through the identification of the physical locations where the velocity vanishes (i.e. critical points), the behaviour of the streamlines in the vicinity of these points and the manner in which the critical points are connected by the streamlines. No-slip critical points are defined as points where the slope of the streamlines is undetermined on a solid wall. In contrast to free-slip critical points, which are defined as the spatial locations where the three components of the velocity vanish, no-slip critical points are located where the components of the wall-shear are equal to zero. The streamlines very near the solid wall lie closely along curves which remain tangent to the wall-shear, denominated *surface streamlines*, *limiting streamlines* or *skin-friction lines*. The pattern of surface streamlines can be approximately defined using (experimental) oil visualization, which permits direct comparison between theory and experiments.

In line with the curvilinear coordinates introduced for the instability analysis, the orthogonal body-fitted coordinate system is defined where ξ_1 and $z = \xi_3$ are the chordwise and spanwise directions and ξ_2 is the wall-normal coordinate. Within the system of curvilinear coordinates the wall-shear is defined as

$$\frac{\partial \mathbf{v}}{\partial \mathbf{n}} = \gamma \cdot \mathbf{n}, \tag{4}$$

where $\gamma = \tau/\mu$ is the strain tensor and $\mathbf{n} = (0, 1, 0)^T$ the wall-normal direction. The first integral of (4) gives

$$\mathbf{v} = \epsilon \cdot \xi_2. \tag{5}$$

The derivation of the wall-shear is straightforward, resulting in

$$\epsilon = \left(\frac{1}{h_2}\frac{\partial v_1}{\partial \xi_2} + \frac{1}{h_1}\frac{\partial v_2}{\partial \xi_1},\ \frac{2}{h_2}\frac{\partial v_2}{\partial \xi_2},\ \frac{\partial v_2}{\partial \xi_3} + \frac{1}{h_2}\frac{\partial v_3}{\partial \xi_2} \right)^T. \tag{6}$$

No-slip critical points are identified as the locations where $\epsilon = 0$. The trajectories of the surface streamlines can be integrated locally using a Taylor expansion of (5) around a critical point

$$\mathbf{v} = \nabla\epsilon \cdot \xi \cdot \xi_2 + \cdots. \tag{7}$$

The matrix $\mathbf{J} = \nabla\epsilon$ is the Jacobian of the streamlines. In the most general case three planes contain solution trajectories originating at the critical point, defined by the eigenvectors of $\mathbf{J}$. Let λ be the eigenvalues of the $\mathbf{J}$, satisfying the equation

$$\lambda^3 + P\lambda^2 + Q\lambda + R = 0, \tag{8}$$

where P, Q and R are the scalar invariants of $\mathbf{J}$. The incompressibility condition translates into the vanishing of the first invariant, $P = 0$, as for free-slip critical points. If the wall curvature at the critical point is small enough, $\partial h_1/\partial \xi_1$, $\partial h_1/\partial \xi_2$, $\partial h_2/\partial \xi_1$, $\partial h_2/\partial \xi_2 \ll 1$ and the metric functions can be considered constant in the Taylor expansion. In this case differentiation of the continuity equation yields

$$\frac{\partial^2 v_2}{\partial \xi_2^2} \approx -\left(\frac{h_2}{h_1}\frac{\partial^2 v_1}{\partial \xi_1 \partial \xi_2} + h_2 \frac{\partial^2 v_3}{\partial \xi_2 \partial \xi_3} \right). \tag{9}$$

Integrating twice Eq. 9, a second-order approximation is obtained for the wall-normal velocity in the vicinity of the surface

$$v_2 \approx -\left(\frac{h_2}{h_1}\frac{\partial v_1}{\partial \xi_1} + h_2 \frac{\partial v_3}{\partial \xi_3} \right) \cdot \frac{\xi_2^2}{2}, \tag{10}$$

Table 1 Classification of the no-slip critical points on the suction-side wall streamlines

			R	Q	S_1
LE	–	Reattachment	=0	<0	<0
S	–	Separation	=0	<0	<0
R	–	Reattachment	=0	<0	<0
TE	–	Separation	=0	<0	<0
S1	N(s)	Separation	<0	<0	<0
S2	S	Separation	>0	<0	<0
R1	S	Reattachment	<0	<0	<0
R2a	S	Reattachment	<0	<0	<0
R2b	N(u)	Reattachment	>0	<0	<0
R3a	NF(u)	Reattachment	>0	<0	=0
R3b	F(u)	Reattachment	>0	?	>0
R4	S	Reattachment	<0	<0	<0
T1′	N(s)	Separation	<0	<0	<0
R2–R4	NS	Reattachment	=0	<0	<0
S2–R2	NS	–	=0	<0	<0
R1–T1′	NS	–	=0	<0	<0

N node, *S* saddle, *F* focus, *NF* node-focus, *NS* node-saddle, (*s*) stable, (*u*) unstable

which, evaluated at the critical point, determines whether separation or reattachment occurs at the critical point. It should be noted that the limit of (9) and (10) for the case of a flat plate, i.e. $h_1 = h_2 = 1$, is exact. In the present case an airfoil with maximum thickness 15% of the chord is considered, and the assumption of negligible derivatives of the metric function can be not correct. The topological reconstruction performed herein comprises the full equations for curvilinear coordinates, in agreement with the stability analysis, without resort to the flat plate assumption.

The local trajectories of the surface streamlines are obtained as eigensolutions of the linear problem (7). The cubic Eq. 8 can have (i) three different real roots, (ii) all real roots with at least two of them equal, and (iii) a pair of complex roots and one real root. Real and complex solutions are separated in the Q–R space by the curve in which the discriminant of the eigenvalues, i.e. the roots of (7) vanishes (cf. Chong et al. [7]):

$$S_1 = 27R^2 + 4Q^3 = 0. \tag{11}$$

Complex eigenvalues, related to swirling flow regions, are associated with $S_1>0$; in this case the critical point can be a focus or a center. On the other hand, real eigenvalues are associated with $S_1<0$ [7], and the corresponding critical point is then a node/saddle/saddle combination. In addition, the sign of the third invariant, R, determines whether the critical point is attracting streamlines ($R < 0$), in which the critical point is said to be stable, or repelling them ($R > 0$) in which case the point is unstable. The classification of stable or unstable critical points is made on account of the streamlines trajectories, and has no direct relation with the stability behaviour of the flow.

Borderline cases, e.g. $R = 0$ or $S_1 = 0$, are defined as local degeneracies: under an infinitesimal perturbation of the flow the classification of the critical point and the behaviour of the streamlines will change. In order to illustrate this, consider the separation and reattachment lines in the basic flow. The basic flow is two-dimensional and homogeneous in the spanwise direction: the velocity $w = v_3$ and its derivatives with respect to ξ_1 and ξ_2, as well as flow derivatives with respect to $z = \xi_3$ are equal to zero. Consequently, the only non-zero terms in the Jacobian matrix are j_{11}, j_{12}, j_{21} and j_{22}, while the invariant $R = 0$. Separation and reattachment take place in two points (denominated S and R in Table 1) where $j_{12} \sim \partial^2 v_1/\partial\xi_2^2 > 0$ and $j_{21} \sim \partial^2 v_2/\partial\xi_1\partial\xi_2 \sim 0$. At separation the term $j_{11} < 0$ ($j_{11} > 0$ at reattachment) and continuity implies that $j_{11} = -j_{22}$. This critical point has two real eigenvalues with opposite sign, defining a saddle point, and a third eigenvalue $\lambda_3 = 0$, implying that there is no flow in the third eigendirection, i.e. the flow is two-dimensional.

Consider now the Jacobian matrix $\mathbf{J}$ of a three-dimensional flow field constructed by linear superposition of the basic flow and a three-dimensional perturbation with small amplitude $\varepsilon \ll 1$, evaluated at a critical point on the separation line. The total Jacobian of the composite field takes the form

$$\mathbf{J} = \begin{pmatrix} \bar{j}_{11} & \bar{j}_{12} & 0 \\ 0 & \bar{j}_{22} & 0 \\ 0 & 0 & 0 \end{pmatrix} + \varepsilon \begin{pmatrix} \hat{j}_{11} & \hat{j}_{12} & \hat{j}_{13} \\ \hat{j}_{21} & \hat{j}_{22} & \hat{j}_{23} \\ \hat{j}_{31} & \hat{j}_{32} & \hat{j}_{33} \end{pmatrix}, \tag{12}$$

where the elements $\bar{j}_{ij}$ correspond to the basic flow and $\hat{j}_{ij}$ correspond to the perturbation. The characteristic polynomial (Eq. 8) for the perturbed flow is

$$-\lambda^3 - \lambda\, \bar{j}_{11} \cdot \bar{j}_{22} + \varepsilon \left\{ \lambda^2 + \bar{j}_{11} \cdot \bar{j}_{22} \cdot \hat{j}_{33} \right\} + \cdots = 0, \tag{13}$$

and for consistency with the linear analysis higher-order terms on ε are not retained. Considering only the order unity terms, the real eigenvalues $\lambda_{1,2} = \pm\sqrt{\bar{j}_{11} \cdot \bar{j}_{22}}, \lambda_3 = 0$ are obtained. The ε-order terms affect the eigenvalues λ_1 and λ_2 as linearly-small corrections; however now $\lambda_3 = \varepsilon \hat{j}_{33} \neq 0$ and, as a consequence, $R \neq 0$. The classification of the critical point changes from the degenerate two-dimensional saddle point to a three-dimensional node-saddle-saddle point, regardless of the disturbance amplitude ε. The classification of the critical points appearing throughout the paper according to the surface streamlines and the location on the R–Q space is shown in Table 1. In the same table the nature of all critical points which appear in the analysis of the next section is defined.

3 Results

Instability analyses were performed for the basic flow corresponding to an airfoil at angle of attack of 18° and a chord-length Reynolds number $Re = 200$. Under these conditions the two-dimensional flow is steady and laminar, separating downstream of the leading edge, immediately after the leading-edge suction peak. The algorithm discussed in [14,19] has been used. The convergence of the eigenspectrum window containing the most unstable eigenvalues required the use of 249 × 250 collocation points. Owing to the dense linear algebra operations employed, the discretized matrix requires $\mathcal{O}(1)$ Terabyte of distributed memory for its storage, while computation of a Krylov subspace of dimension $m_{\text{Kryl}} \approx 1000$ takes $\mathcal{O}(24)$ h of wall-time on 1024 processors of the Mare Nostrum computing facility (www.bsc.es); the same computation on 2048 processors of the Blue Gene/P facility at the Forschungszentrum Jülich (www.fz-juelich.de) requires $\mathcal{O}(12)$ h of wall-time for each wavenumber parameter value, β. The computational domain used extends 16 chords in the wall-normal direction, although convergence of the eigenvalue corresponding to the leading stationary eigenmode is obtained with a shorter domain extension of 11 chords in this direction. The eigenspectrum corresponding to $\beta = 1$ is shown in Fig. 1. The eigenmodes evolving in time with an exponential dependence on the eigenvalue, the eigenmode with the largest amplification rate, i.e. largest imaginary part, will dominate the long-time behaviour of the flow. The leading eigenmode is unstable, stationary ($\omega_r = 0$), and three-dimensional ($\beta \neq 0$). The spatial structure of the amplitude functions relates it to the global mode which has been found consistently in three-dimensional BiGlobal instability analysis of laminar separation bubble flows on flat plates [24,26], backsteps [3], bumps [10], low-pressure-turbines [1] and S-shaped ducts [16]: the peak of the dominant streamwise disturbance velocity component is attained just downstream of the maximum recirculation region in the basic flow, while a spanwise disturbance velocity component exists and is responsible for the three-dimensionalization of the basic state. The nature and topological bifurcations exerted by this global mode on the steady two-dimensional flow will be the subject of the analysis presented in the next sections.

3.1 Topological changes exerted by the stationary global mode

The two-dimensional basic flow shown in the left part of Fig. 2 as a three-dimensional extension on the $O\xi_1\xi_3$ half-plane (since the bifurcations to be shown in what follows are periodic in $z = \xi_3$) can be described by means of four no-slip critical points on the airfoil surface and three free-slip critical points defining the recirculation region. The four no-slip critical points at the wall correspond to the attachment point near the leading edge (LE), the separation point on the suction side (S), the reattachment point on the pressure side (R) and the detachment point on the trailing edge (TE). Due to the two-dimensionality of the flow, the loci of these critical points on different spanwise vertical planes give rise to the lines denoted as *Leading edge*, *Separation line*, *Reattachment line* and *Trailing edge* on the left part of Fig. 2, all of which are at right angles to the oncoming stream. The flow being homogeneous in the spanwise direction, the only non-zero terms in the Jacobian matrix $\mathbf{J}$ are j_{11}, j_{12}, j_{21} and j_{22}, while the invariant $R = 0$. This topology is defined as structurally unstable, as an arbitrarily small three-dimensional disturbance will give rise to a new topology, as was shown in sect. 2.3. In the general case, the spanwise component of the wall-shear will vanish only at certain locations, where discrete critical points will emerge, as opposed to the separation and reattachment lines. The perturbed Jacobian will

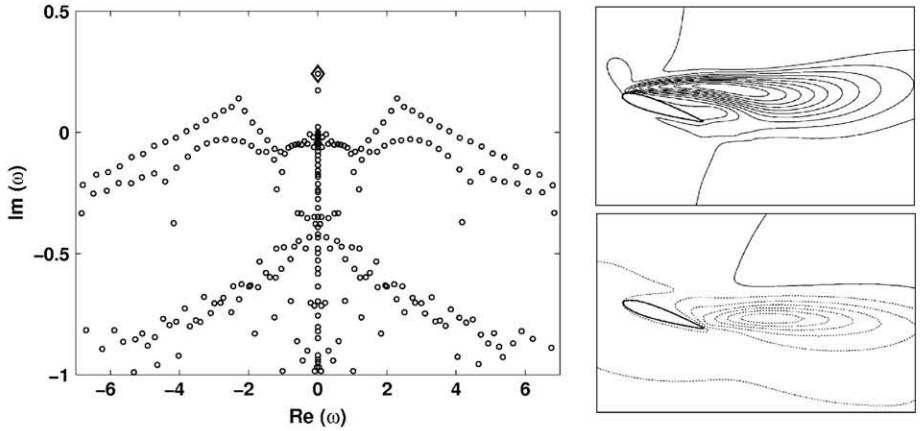

Fig. 1 *Left*: eigenvalue spectrum at $\beta = 1$; the eigenvalue highlighted with a diamond corresponds to the most unstable stationary global mode. *Right*: amplitude functions of the most unstable eigenmode at $\beta = 1$. *Up*: streamwise velocity component $\hat{u}$ on the plane $z\beta = 0$; the contours shown are $[-0.9(0.1)0.9]$. *Down*: spanwise velocity component $\hat{w}$ on the plane $z\beta = \pi$; the contours shown are $[-0.9(0.1) - 0.1)]$

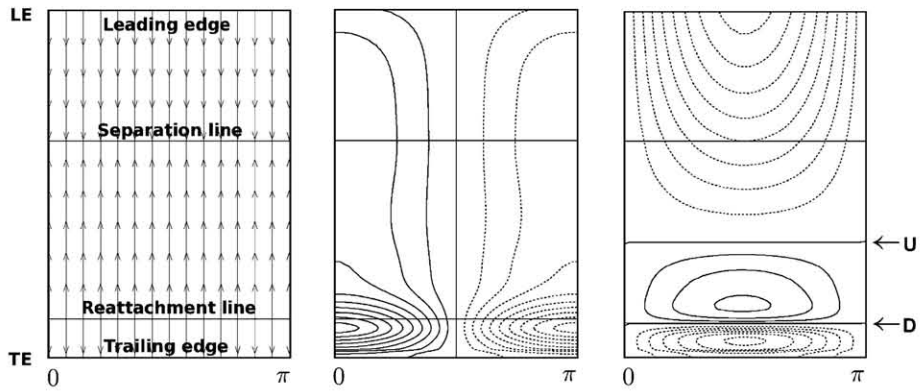

Fig. 2 Topology of the basic flow (*left*), and the chordwise (*middle*) and spanwise (*right*) components of the perturbation wall-shear. The contours of the chordwise component are $[-0.9(0.1)0.9]$. The contours of the spanwise component are $[-0.9(0.1)-0.1]$ (*dashed*) and [0 (0.05) 0.15] (*solid*)

then become inhomogeneous in the spanwise direction, and $R \neq 0$. The different topologies on the surface streamlines generated by the linear superposition of the basic flow and the most unstable stationary global mode for the spanwise wavenumber $\beta = 1$, corresponding to a periodicity length of $L_z = 2\pi$, are studied in detail in what follows.[1]

The amplitude functions of the eigenmode are normalized to have maximum velocity component equal to unity, and are then multiplied by a certain amplitude $\varepsilon \ll 1$, previously to being superposed to the two-dimensional basic flow, in line with decomposition (1). The resulting flow pattern is rather involved, and the description of the three-dimensional streamlines in three-dimensional space could become blurred. The present paper is focused on the topology of the surface streamlines only, and consequently only the no-slip critical points of the reconstructed flow are considered. The classification of the critical points appearing along the paper is summarized in Table 1.

The components of the wall-shear induced by the amplitude functions of the global eigenmode (shown in Fig. 1, right) are also depicted in Fig. 2. Taking into account the periodicity in the spanwise direction, only half spanwise period ($\beta z \in (0, \pi)$) is shown. The selection of the initial phase being arbitrary, $\beta z = 0$ has been set where the spanwise wall-shear component vanishes. The chordwise component has a constant sign at each z-plane, decelerating the flow in $\beta z \in (0, \pi/2)$ and accelerating it in $\beta z \in (\pi/2, \pi)$. The consequence

[1] The wavenumber parameter chosen to be analysed is representative of all unstable flows obtained, including $\beta \approx 2$ at which the most unstable flow is encountered at $Re = 200$, $AoA = 18°$; note that $\beta \approx 2$ corresponds to stall cell spanwise periodicity length of $L_z \approx \pi$.

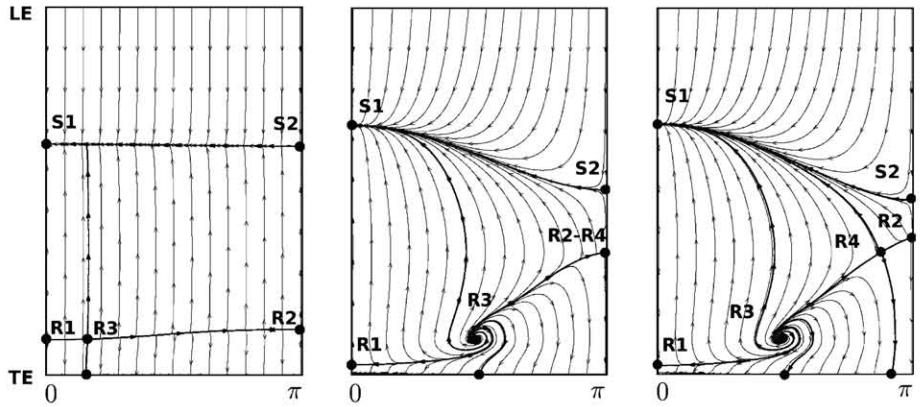

Fig. 3 First topology bifurcation: evolution from topology 1 (*left*) to topology 2 (*right*) through borderline case 1 (*center*)

of the acceleration (deceleration) is a local reduction (increment) of the total reversed flow region, displacing the critical points along the chord. The spanwise wall-shear component acts in counter-phase to the chordwise component, vanishing at $\beta z = 0$, and $\beta z = \pi$. In addition, the spanwise wall-shear component vanishes at two further chordwise locations as shown in Fig. 2, right; these locations will be referred to as U (for upstream) and D (for downstream) in what follows. The location and classification of the critical points vary proportionally to the reconstruction amplitude ε, and accordingly one can reconstruct the path of topological bifurcations that the flow field will undergo in the presence of the temporally amplified global eigenmode.

The geometry of the airfoil introduces a new issue to the surface streamlines topology of separated flow, in comparison to its flat-plate counterpart [20]. The Kutta condition imposes flow stagnation at both the leading edge and the trailing edge. Therefore, any point on those lines remains a critical point in three-dimensional flow; both LE and TE then serve as origin or end of dividing streamlines, i.e. streamlines connecting critical points.

3.1.1 Topology 1, leading to borderline case 1

Figure 3 shows a sequence of events described below as the progression from Topology 1 to Topology 2, via Borderline Case 1. In the case of a perturbation of infinitesimal amplitude being superposed upon the degenerate two-dimensional basic flow, the latter is replaced by a fully three-dimensional flow field, which is described by a set of critical points. No-slip critical points appear at the locations where the wall-shear components vanish: these locations are the intersections of the separation and reattachment lines of the basic flow with the lines $\beta z = 0$ and $\beta z = \pi$, where the spanwise disturbance component of the wall-shear vanishes. The resulting critical points are denoted as S1, S2 (for separation) and R1, R2 (for reattachment). The separatrices, i.e. streamlines connecting these critical points, are reminiscent of the separation and reattachment lines of the basic flow, and practically overlap with the lines defining vanishing of the chordwise component of the total wall-shear. In accordance, these separatrices will be also referred to as separation and reattachment lines in the three-dimensional flow reconstructions. A third critical point (R3) appears along the reattachment line, at the location where the spanwise component of the wall-shear vanishes (line D). When the disturbance amplitude $\varepsilon \to 0$, R3 approximates a degenerate unstable node-focus (R3a); at any finite but small perturbation amplitude R3 is an unstable focus (R3b).

The total flow pattern, i.e. the description of the critical points and connecting streamlines, will remain topologically equivalent until certain finite disturbance amplitude, ε_1, has been attained; in the present reconstruction $\varepsilon_1 \approx 2.49 \cdot 10^{-3}$. This is the amplitude associated with the first bifurcation, identified as the situation when R2 reaches the upstream change-of-sign of the spanwise wall-shear component (line U). At this instant, the invariant $R = 0$, and the flow is locally two-dimensional in the vicinity of R2: the critical point R2 becomes a degenerate node-saddle point, and is identified here as R2–R4. This borderline topology defines a bifurcation of the surface streamlines: an arbitrarily small increase in $\varepsilon > \varepsilon_1$ will result in the Topology 2, described below.

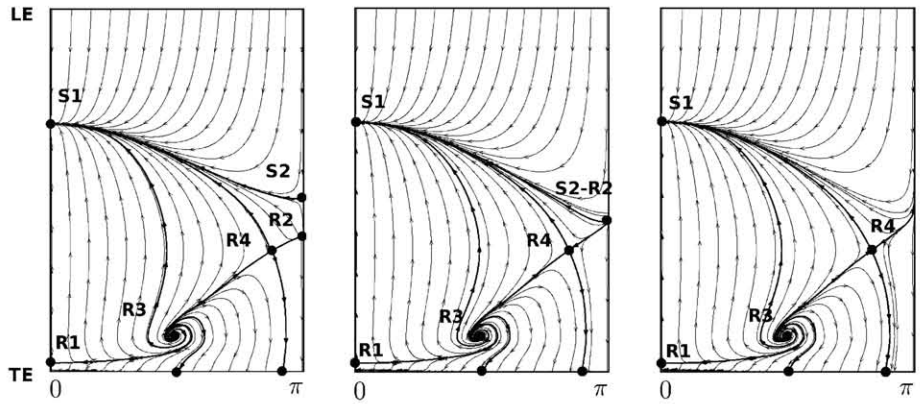

Fig. 4 Second topology bifurcation: evolution from topology 2 (*left*) to topology 3 (*right*) through borderline case 2 (*center*)

3.1.2 Topology 2, leading to borderline case 2

The evolution between Topologies 2 and 3 through Borderline Case 2 is shown in Fig. 4. The degenerate critical point R2–R4 now splits into two independent critical points when $\varepsilon > \varepsilon_1$. One critical point remains at $\beta z = \pi$ and becomes an unstable node (R2b). The other critical point becomes a saddle point, denoted by R4, and remains at the location of vanishing spanwise wall-shear component (line U). The reattachment line continues connecting R2b, R4, R3 and R1. However, the saddle point R4 is connected with the separation point S1 and with the trailing edge (TE); two independent but adjacent reversed flow regions (S1–R1–R3–R4–S1 and S1–R4–R2b–S2–S1) are present now. The physical interpretation of this topological change is the *loss of connectivity of the original reverse flow*. This change will later lead to the spanwise periodic breakdown of the initially two-dimensional reversed flow region.

A new topological bifurcation appears when the disturbance amplitude $\varepsilon_2 \approx 2.835 \cdot 10^{-3}$ is attained, as the critical points S2 and R2b coalesce. The resulting degenerate point S2–R2 is a node-saddle: and the flow is again locally two-dimensional with $R = 0$. This topology, denominated Borderline Case 2, defines the bifurcation in which one of the reversed flow regions (S1–R4–R2b–S2–S1) disappears and a new Topology 3 appears.

3.1.3 Topology 3, leading to borderline case 3

The evolution of Topology 3 through the bifurcation denoted as Borderline Case 3 to Topology 4 is shown in Fig. 5. When $\varepsilon > \varepsilon_2$ the degenerate critical point S2–R2 disappears. With the disappearance of the second reversed flow region, spanwise sections appear in which the flow is entirely attached; the periodic breakdown of the separated region has been completed and reconnections of the dividing streamlines have resulted. The separatrices connecting S1–R4 and R4–R3 are reminiscent of the separation and reattachment lines, respectively, and enclose the reversed flow region. The streamline previously connecting the leading edge (LE) to S2 is connected now to the saddle R4. In addition, a direct connection exists between the leading edge and the trailing edge at $\beta z = \pi$, ensuring spanwise symmetry of the flow.

With a further increase of the disturbance amplitude, a new critical point T1′ emerges from the trailing edge and moves upstream. A secondary separated region appears, delimited by the streamline connecting T1′ to TE. Eventually T1′ and R1 coalesce into the degenerate node-saddle point R1–T1′, resulting into a new topology bifurcation, denominated Borderline Case 3. In the present reconstruction this phenomenon appears when the disturbance amplitude is $\varepsilon_3 \approx 4.58 \cdot 10^{-3}$.

3.1.4 Topology 4

The degenerate point R1–T1′ disappears when the disturbance amplitude is higher than ε_3 and the flow attains non-linear levels. The main reversed flow region and the secondary separated region connect for the first time. The streamline formerly connecting R3 to R1 connects now R3 to S1, and a direct connection appears between S1 and the trailing edge. The resulting topology describes independent reversed flow regions which extend from the separation saddle S1 to the trailing edge; the surface streamlines in these reversed flow regions emerge

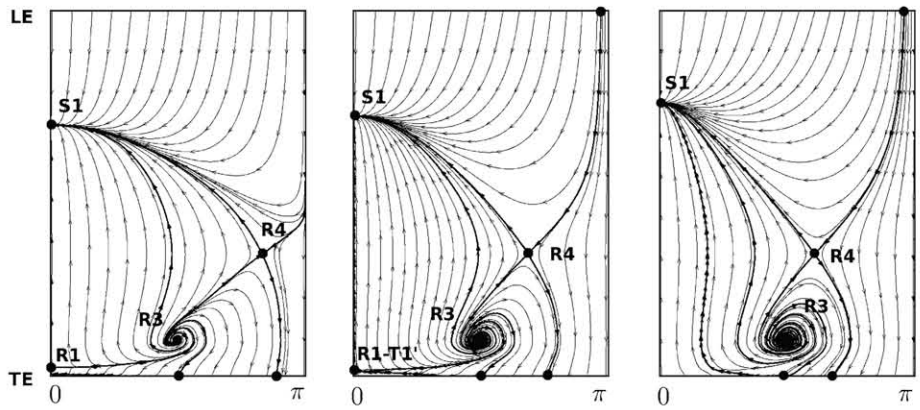

Fig. 5 Third topology bifurcation: evolution from topology 3 (*left*) to topology 4 (*right*) through borderline case 3 (*center*)

from two counter-rotating foci, and lead to a *flow pattern topologically identical to the stall cells observed experimentally*. A three-dimensional image of the flowfield resulting from superposition of the basic flow and the leading global eigenmode at amplitudes $\varepsilon > 5 \times 10^{-3}$ is shown in Fig. 6.

4 Discussion

The steady two-dimensional flow around a stalled airfoil at Reynolds number $Re = 200$ supports an intrinsic three-dimensional modal linear instability mechanism, recovered here as the leading global eigenmode of the massively separated flow. Multiple surface streamline topologies are generated by linear superposition to the two-dimensional basic flow of this global mode at increasingly large (but small enough to be considered linear) disturbance amplitudes. In the three-dimensional reconstructions performed herein, topological bifurcations occur at disturbance amplitudes $\varepsilon \sim \mathcal{O}(10^{-3})$, levels at which the linearization hypothesis is still valid. Since the leading global eigenmode is unstable at the conditions monitored, the perturbation amplitude will grow exponentially and the flow field will undergo all the topology bifurcations described herein, until non-linear effects will appear and saturate further growth. Similar stall-cell structures have been shown to exist in a laminar separation bubble embedded in adverse-pressure-gradient boundary-layers over a flat plate [20]. There too the origin of the topological changes lies with the global flow eigenmode. While in terms of amplitude function structures the leading eigenmodes of separated flow on the flat plate and the stalled wing share their principal characteristics, a result established through research on other types of airfoils and low-pressure-turbines [27,1], the absence of the trailing edge in the flat plate is responsible for the differences in the respective surface streamlines topology.

The three-dimensional composite flow fields resulting from two disturbances amplitudes, one before the first topological bifurcation appears ($\varepsilon < \varepsilon_1$) and one after the last topological bifurcation ($\varepsilon > \varepsilon_3$), are shown in the Fig. 6. A spanwise waviness of the vortex cores (highlighted as the red lines in the figure), in perfect qualitatively agreement with the model of Weihs and Katz [29], is attained in the case of the low-amplitude reconstruction. The streamlines (black lines) show the three-dimensionalization of the flow exerted by the global mode; closed recirculation regions no longer exist and the streamlines are initially attracted into the vortex core, around which they seem to wind before they are finally repelled and trail downstream. In the higher-amplitude reconstruction the line corresponding to the upper vortex core is broken periodically in the spanwise direction, extending downstream, in a pattern similar to the one proposed by Yon and Katz [31]. The criterion employed for the detection of the vortex cores, namely the identification of local maxima of Q, the second invariant of the velocity gradient tensor, indicates that the vortex only continues downstream for a short distance. Accordingly, no focal points are found in the cross-sectional planes, and the three-dimensional streamlines do not exhibit a swirling motion in the wake. Though rather speculative, the rapid dissipation of the streamwise vortices is attributed to the extremely low Reynolds number, compared to the experimental values.

The surface streamlines corresponding to the higher-amplitude reconstruction in Fig. 6 as was shown in the previous section are strongly reminiscent of the experimental oil-streak visualizations. The precise topological description, i.e. critical points and connecting streamlines, of the experimental *owl-faces* cannot be

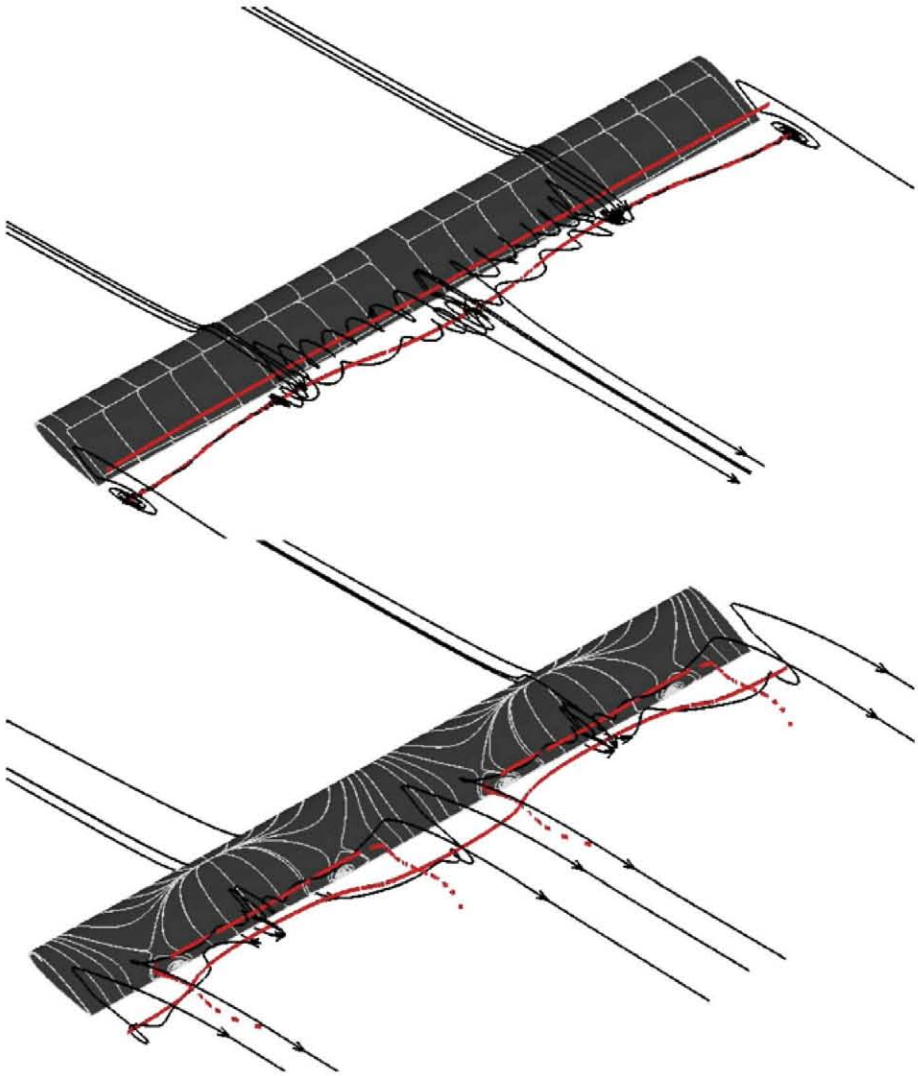

Fig. 6 Three-dimensional reconstructions of the flow field generated by the linear superposition to the two-dimensional basic flow around a stalled airfoil of its leading stationary three-dimensional eigenmode with amplitudes $\varepsilon = 10^{-4}$ (*up*) and $\varepsilon = 5 \cdot 10^{-3}$ (*down*). Graphically superposed are streamlines (*black lines*), surface streamlines (*light grey*) and vortex cores (*red lines in the online paper version*) identified as local maxima of Q, the second invariant of the velocity gradient tensor

determined, on account of the unsteady behaviour of the experimental stall cells, where the oil-streaks are only a time-averaged representation of the surface streamlines. The flow unsteadiness observed experimentally in tunnel experiments under Reynolds number $\sim \mathcal{O}(10^5)$ has been suggested [31] to be caused by phenomena coexisting with the stall cells, in particular instabilities of the shear layer, but not causally related to them. In their experimental measurements Yon and Katz identified different frequencies on the pressure signal, one related to the wake instability ($St \approx 0.15$) and another with high amplitude and low frequency $St \approx 0.04$. Both Yon and Katz [31] and Zaman et al. [32] concluded independently that the low frequency fluctuations are related to a violent motion of the leading edge shear-layer, termed *shear-layer flapping*, resulting from a transitional or turbulent state of the separated shear-layer. Here, the oscillatory behaviour of the flow could be explained in the context of a modal linear instability analysis with the inclusion of the other less-amplified but still unstable oscillatory modes that were recovered in the BiGlobal instability analysis (see Fig. 1, left), and that where not considered in the topology reconstruction leading to the stall cells. The most unstable travelling ($\omega_r \neq 0$) eigenvalues in the spectrum shown in Fig. 1 have dimensionless frequency $\omega_r \approx 2.293$. The Strouhal number based on the frontal projected height of the pitched-up airfoil is $St = \omega_r/(2\pi) \cdot \sin 18^\circ \approx 0.11$, somewhat lower but of the same order as the $St \approx 0.15$ of the fast oscillations associated with the wake instability.

On the other hand, the absence of an explanation for the low-frequency flapping in the present laminar flow reconstruction is in line with the conclusion of Zaman et al. [32] and Yon and Katz [31], who related it to turbulent shear-layers.

5 Concluding remarks

The effect of the amplification of the three-dimensional global mode of laminar separation on the wing is to generate three-dimensional modulation in the spanwise spatial direction as well as to alter the extension in the basic state of the connex region of reversed flow. The latter eventually breaks down to periodic cells having a spanwise periodicity length predicted by global linear instability theory. This spanwise periodic breakdown gives rise to independent stationary separated flow regions, in which the structure of the streamlines is organized around two counter-rotating foci. The present quantitative description of the flow field topology, as one of a steady laminar two-dimensional flow perturbed by its leading unstable global eigenmode, puts for the first time on a firm theoretical basis the multitude of phenomenological descriptions of the stall cells observed in experiments on airfoils close to and beyond stall [5,21,29–31].

Acknowledgements The material is based upon work sponsored by the Air Force Office of Scientific Research, Air Force Material Command, USAF, under Grant number # FA8655-06-1-3066 to *nu modelling s.l.*, entitled *Global instabilities in laminar separation bubbles*. The Grant is monitored by Dr. D. Smith of AFOSR (originally by Lt. Col. Dr. Rhett Jefferies) and Dr. S. Surampudi of EOARD. The views and conclusions contained herein are those of the author and should not be interpreted as necessarily representing the official policies or endorsements, either expressed or implied, of the Air Force Office of Scientific Research or the U.S. Government. Computations have been performed on the CeSViMa (www.cesvima.upm.es), MareNostrum facilities (www.bsc.es) and DEISA-*Forschungszentrum Jülich* (www.deisa.com). The authors are grateful to Dr. V. Kitsios and Prof. J. Soria for providing the basic flow analysed. Discussions with Prof. H. Fasel on the appearance of stall cells in flight are kindly acknowledged.

References

1. Abdessemed, N., Sherwin, S.J., Theofilis, V.: Linear instability analysis of low pressure turbine flows. J. Fluid Mech. **628**, 57–83 (2009)
2. Allen, T., Riley, N.: Absolute and convective instabilities in separation bubbles. Aeronaut. J. **99**, 439–448 (1995)
3. Barkley, D., Gomes, M.G.M., Henderson, R.D.: Three-dimensional instability in a flow over a backward-facing step. J. Fluid Mech. **473**, 167–190 (2002)
4. Bippes, H., Turk, M.: Windkanalmessungen in einem Rechteckflügel bei anliegender und abgelöster Strömung. Tech. rep., DFVLR Forschungsbericht IB 251-80 A 18 (1980)
5. Bippes, H., Turk, M.: Half model testing applied to wing above and below stall. In: Recent Contributions to Fluid Mechanics, pp. 22–30. Springer-Verlag, New York (1982)
6. Chomaz, J.M., Huerre, P., Redekopp, L.G.: Bifurcation to local and global modes in spatially developing flows. Phys. Rev. Lett. **60**, 25–28 (1988)
7. Chong, M.S., Perry, A.E., Cantwell, B.J.: A general classification of three-dimensional flow fields. Phys. Fluids **2**(5), 765–777 (1990)
8. Dallmann, U.: Topological structures of three-dimensional flow separations. DFVLR-IB 221-82 A07 (1982)
9. Dallmann, U.C., Vollmers, H., Su, W.H.: Flow topology and tomography for vortex identification in unsteady and in three-dimensional flows. In: IUTAM Symposium on Simulation and Identification of Organized Structures in Flows, Lyngby, Denmark, pp. 223 – 238 (1997)
10. Gallaire, F., Marquillie, M., Ehrenstein, U.: Three-dimensional transverse instabilities in detached boundary-layers. J. Fluid Mech. **571**, 221–233 (2007)
11. Hammond, D.A., Redekopp, L.G.: Local and global instability properties of separation bubbles. Eur. J. Mech. B/ Fluids **17**, 145–164 (1998)
12. Hornung, H.G., Perry, A.E.: Some aspects of three-dimensional separation. Part I streamsurface bifurcations. Z. Flugwiss. Weltraumforsch **8**, 77–87 (1984)
13. Huerre, P., Monkewitz, P.A.: Local and global instabilities in spatially developing flows. Ann. Rev. Fluid Mech. **22**, 473–537 (1990)
14. Kitsios, V., Rodríguez, D., Theofilis, V., Ooi, A., Soria, J.: Biglobal stability analysis in curvilinear coordinates of massively separated lifting bodies. J. Comp. Phys. **228**, 7181–7196 (2009)
15. Lighthill, M.J.: Attachment and Separation in three-dimensional flow. In: Rosenhead, L. (ed.) Laminar Boundary Layers, pp. 72–82. Oxford University Press, New York (1963)
16. Marquet, O., Lombardi, M., Chomaz, J.M., Sipp, D., Jacquin, L.: Direct and adjoint global modes of a recirculation bubble: lift-up and convective non-normalities. J. Fluid Mech. **622**, 1–21 (2009)
17. Perry, A.E., Chong, M.S.: A description of eddying motions and flow patterns using critical point concepts. Ann. Rev. Fluid Mech. **19**, 125–156 (1987)

18. Perry, A.E., Hornung, H.G.: Some aspects of three-dimensional separation. Part II vortex skeletons. Z. Flugwiss. Weltraumforsch **8**, 155–160 (1984)
19. Rodríguez, D., Theofilis, V.: Massively parallel numerical solution of the biglobal linear instability eigenvalue problem using dense linear algebra. AIAA J. **47**(10), 2449–2459 (2009)
20. Rodríguez, D., Theofilis, V.: Structural changes induced by global linear instability of laminar separation bubbles. J. Fluid. Mech (2010). doi:10.1017/S0022112010000856
21. Schewe, G.: Reynolds-number effects in flow around more-or-less bluff bodies. J. Wind Eng. Ind. Aerodyn. **89**, 1267–1289 (2001)
22. Surana, A., Grunberg, O., Haller, G.: Exact theory of three-dimensional flow separation. part 1 steady separation. J. Fluid Mech. **564**, 57–103 (2006)
23. Taira, K., Colonius, T.: Three-dimensional flows around low-aspect-ratio flat-plate wings at low reynolds numbers. J. Fluid Mech. **623**, 187–207 (2009)
24. Theofilis, V.: Global linear instability in laminar separated boundary layer flow. In: Fasel, H., Saric, W. (eds.) Proceeding of the IUTAM Laminar-Turbulent Symposium V, pp. 663 – 668. Sedona, AZ, USA (2000)
25. Theofilis, V.: Advances in global linear instability of nonparallel and three-dimensional flows. Prog. Aero. Sci. **39**(4), 249–315 (2003)
26. Theofilis, V., Hein, S., Dallmann, U.: On the origins of unsteadiness and three-dimensionality in a laminar separation bubble. Phil. Trans. R. Soc. Lond. A **358**, 3229–3246 (2000)
27. Theofilis, V., Barkley, D., Sherwin, S.J.: Spectral/hp element technology for flow instability and control. Aero. J. **106**, 619–625 (2002)
28. Tobak, M., Peake, D.: Topology of three-dimensional separated flows. Annu. Rev. Fluid Mech. **14**, 61–85 (1982)
29. Weihs, D., Katz, J.: Cellular patterms in poststall flow over unswept wings. AIAA J. **21**(12), 1757–1759 (1983)
30. Winkelmann, A., Barlow, B.: Flowfield model for a rectangular planform wing beyond stall. AIAA J. **8**, 1006–1008 (1980)
31. Yon, S.A., Katz, J.: Study of the unsteady flow features on a stalled wing. AIAA J. **36**(3), 305–312 (1998)
32. Zaman, K.M.B.Q., McKinzie, D.J., Rumsey, C.L.: A natural low-frequency oscillation of the flow over an airfoil near stalling conditions. J. Fluid Mech. **202**, 403–442 (1989)